Supplementary Material

Mechanistic Evaluation of Static and Dynamic Adsorption of Brassica juncea Derived Gemini Surfactants: Implications to Enhanced Oil Recovery

Lavisha Jangid, Keka Ojha, Ajay Mandal*

Enhanced Oil Recovery & Carbon Utilization and Storage (EOR&CUS) Lab
Department of Petroleum Engineering, Indian Institute of Technology (Indian School of Mines), Dhanbad -826004, India

* Corresponding Author, email: ajay@iitism.ac.in

S.1. XRD Analysis

The X-ray diffraction (XRD) analysis of reservoir rock is essential in EOR to determine the mineralogical composition, especially reactive clays and carbonates, which significantly influence rock-fluid interactions such as wettability alteration, chemical reactivity, and adsorption behaviour [1]. This understanding helps optimize chemical formulations, predict potential formation damage, and improve oil recovery efficiency by tailoring EOR strategies to specific rock types. XRD patterns of sandstone and carbonate rocks showing relative intensity versus two-theta (2θ) peaks are presented in Fig. S1 (a) and (b) respectively. XRD analysis of the sandstone samples reveals quartz (Qz) as the predominant mineral, comprising approximately 99% of the composition, confirming their classification as sandstone. Quartz, also known as silicon dioxide, crystallizes in a hexagonal crystal system with a measured density of 2.65 g/cm³ in its inorganic form. The iron-bearing mineral hematite (Fe_2O_3) is present in about 1% of the sample, exhibiting a rhombohedral crystal structure with a measured density of 5.27 g/cm³ in its inorganic form. Additionally, minor minerals including kaolinite (Ka), feldspar (Fs), microcline (Mi), and muscovite (Mu) are detected in very few amounts [2]. In contrast, the carbonate rock samples primarily consist of calcite ($CaCO_3$). XRD patterns confirmed characteristic peaks corresponding to calcite as the dominant phase. Trace amounts of quartz and hematite are also detected in the carbonate samples. Semi-quantitative analysis indicates that calcite constituted approximately 98% of the mineral content in the carbonate rocks, crystallizing in a rhombohedral crystal system with a measured density of 2.71 g/cm³. Quartz and hematite each account for approximately 1%, with quartz in a hexagonal crystal system and hematite in a rhombohedral crystal system, having measured densities of 2.65 g/cm³ and 5.27 g/cm³, respectively. This mineralogical composition is typical of carbonate rocks,

specifically limestone, where calcite predominates as the primary constituent. Understanding these mineral phases is critical as they significantly influence the porosity and permeability of the rock, crucial parameters in core flooding and wettability studies.

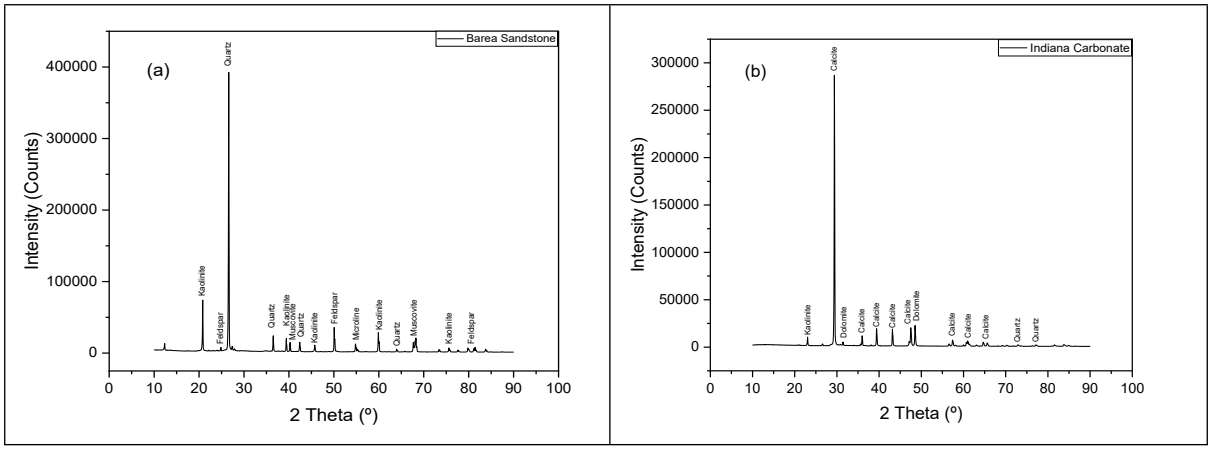

Fig. S1: X-ray diffraction patterns of (a) Barea sandstone; (b) Indiana carbonate

S.2. XRF Analysis

The XRF data in Table S1 show that the elemental composition of the rock sample that there is a high 88.1% SiO_2 mass percentage in the sandstone sample, which indicates that quartz is the predominant element. Feldspar or clay minerals are also present in the sample according to the presence of aluminosilicates with a moderate 7.2% Al_2O_3 amount. Low Fe_2O_3 content of around 1.8% indicates minimal iron-bearing minerals, possibly hematite or limonite, which can influence the rock's colouration and weathering properties. K_2O with a low 1.79% mass composition indicates the presence of potassium feldspar (orthoclase or microcline). MgO, CaO, and Na_2O contents present in a very low amount reflect a silicate-dominated matrix with minimal carbonate minerals or alkali-rich phases [3,4].

In the carbonate, CaO is present in the maximum amount of 93% indicates that the carbonate rock is primarily composed of calcium carbonate minerals like calcite or aragonite. Low SiO_2 content of 2.56% suggests that the carbonate is not significantly mixed with silicate impurities. Moderate 3.64% Fe_2O_3 content indicates the presence of iron-bearing minerals, possibly siderite or iron oxides, which can affect the rock's colour and strength. Low Al_2O_3 and K_2O contents suggest minimal aluminosilicate or feldspar content, consistent with a pure carbonate composition. MgO content of 0.39% suggests minor dolomite or magnesium-bearing impurities [3,5].

Table S1: Metal Oxide Composition Present in the Sandstone and Carbonate Determined by XRF

Sample	*Composition mass%*									
	Na_2O	MgO	Al_2O_3	SiO_2	P_2O_5	K_2O	CaO	TiO_2	MnO	Fe_2O_3
Sandstone	0.2018	0.2033	7.1738	88.0824	0.0376	1.7879	0.0766	0.5492	0.0456	1.8418
Carbonate	0.0257	0.3909	0.2494	2.5566	0.0402	0.059	93.0203	0	0.0209	3.637

S.3. Static Adsorption Isotherm Modelling

To evaluate the adsorption behaviour, such as surface properties, adsorption mechanism, and nature of intermolecular interactions between adsorbate molecules and the adsorbent surface at equilibrium, experimental data were fitted to various adsorption isotherm models. In this work, various adsorption isotherm models have been analysed, including the Linear, Langmuir, Freundlich, Redlich–Peterson, and Hill Isotherm models.

S.3.1 Linear Adsorption Isotherm

The linear adsorption represents the Henry's law behaviour, which assumes a direct proportionality between the amount adsorbed (q_e) and the equilibrium concentration (C_e), as shown in Equation 1:

$$q_e = K_H C_e + C \tag{S1}$$

Where, q_e (mg/g) is the adsorption capacity/amount at equilibrium, C_e (mg/L) is the equilibrium concentration, K_H is the Henry's law constant, and C is a constant. This model is generally applicable to dilute systems and provides a baseline comparison for more complex models.

S.3.2. Langmuir Adsorption Isotherm

The Langmuir isotherm model assumes that the adsorption is a monolayer on a homogeneous surface with a finite number of homogeneous sites, which was originally proposed by Irving Langmuir in 1916, for solid-gas phase bio sorbents [6]. It also assumes that there is no interaction between adsorbed molecules, as shown in the Equation 2:

$$q_e = \frac{q_o K_L C_e}{K_L C_e + 1} \tag{S2}$$

Where, q_e (mg/g) is the adsorption capacity at equilibrium, C_e (mg/L) is the equilibrium concentration, q_o (mg/g) is the maximum adsorption capacity corresponding to complete monolayer coverage, and K_L (L/mg) is the Langmuir constant, which is related to binding

affinity. A higher K_L value indicates stronger solute–adsorbent interactions. The model is widely used to describe chemisorption.

S.3.3 Freundlich Isotherm

The Freundlich isotherm model, which was proposed by Freundlich in 1906, describes adsorption onto heterogeneous surfaces with the possibility of multilayer adsorption. It was the earliest model to establish a relationship for non-ideal and reversible sorption processes [7], as shown in Equation 3:

$$q_e = K_F C_e^{\frac{1}{n}} \tag{S3}$$

Where, q_e (mg/g) is the adsorption capacity at equilibrium, C_e (mg/L) is the equilibrium concentration, K_F (L/mg) is the adsorption capacity, and 1/n indicates the surface heterogeneity. If the value of 1/n is less than 0.5, it signifies favourable adsorption, while the value of 1/n is greater than 0.5, it suggests cooperative adsorption.

S.3.4. Redlich-Peterson Isotherm

The Redlich–Peterson isotherm model is a hybrid model incorporating features of both Langmuir and the Freundlich isotherms proposed by Redlich and Peterson in 1959. Because of this hybrid nature, it can be used in both homogeneous and heterogeneous systems [8], as shown in Equation 4:

$$q_e = \frac{K_R C_e}{1 + \alpha_r C_e^{\beta_r}} \tag{S4}$$

Where, q_e (mg/g) is the adsorption capacity/amount at equilibrium, C_e (mg/L) is the equilibrium concentration, K_R (L/gm) is the Redlich–Peterson constant, α_r is a constant, and β_r is an exponent that varies between 0 and 1. This model approaches the Langmuir isotherm if $\beta_r = 1$ and Freundlich isotherm if $\beta_r = 0$.

S.3.5. Hill Isotherm

The Hill isotherm model was developed from a nonideal competitive adsorption isotherm, which describes cooperative adsorption processes in which the binding of one molecule affects the affinity of subsequent molecules [9], as shown in Equation 5:

$$q_e = \frac{q_{SH} C_{eq}^{n_H}}{K_D + C_{eq}^{n_H}} \tag{S5}$$

Where, q_e (mg/g) is the adsorption capacity at equilibrium, C_e (mg/L) is the equilibrium concentration, q_{SH} (mg/gm) is the maximum binding capacity, K_D is the dissociation constant, and n_H is the Hill coefficient. A Hill coefficient value greater than unity indicates positive cooperativity, a value less than unity indicates negative cooperativity, and a value equal to unity indicates non-cooperative binding.

S.4 Adsorption Kinetics

These models play a critical role in determining the efficiency of the sorption process. The Pseudo-first order model describes physisorption with initial adsorption stages, while the Pseudo-second order model highlights the interaction between adsorbate and adsorbent [10]. The intraparticle diffusion model by Weber and Morris determines the diffusion on the pore scale with the boundary layer effect of diffusion [11]

S.4.1. Pseudo-First Order

The Pseudo-First order model assumes that the rate of adsorption site occupation is directly proportional to the number of unoccupied sites, which is also known as the Lagergren model. This model is often applied for physisorption processes during the early stages of adsorption [12]. The linearized form of the model is shown in Equation 6:

$$\ln\left(q_e - q_t\right) = \ln\left(K_1 q_e\right) - K_1 t \tag{S6}$$

Where, q_e (mg/g) and q_t (mg/g) are the adsorption capacities at equilibrium and at time t (hr), respectively, and K_1 (hr^{-1}) is the pseudo-first-order rate constant.

S.4.2. Pseudo-Second Order

The pseudo-second order model assumes that the adsorption process follows second-order kinetics with respect to the number of unoccupied sites, and it is particularly suited for chemisorption involving valence forces or electron sharing/exchange between adsorbent and adsorbate [13]. The linearized form is expressed as in Equation 7:

$$\frac{t}{q_t} = \frac{1}{K_2 q_e^2} + \frac{t}{q_e} \tag{S7}$$

Where, K_2 (g/mg·hr) is the pseudo-second order rate constant. The model provides better applicability in many systems where chemisorption is the rate-limiting step.

S.4.3. Intraparticle Diffusion Model

The intraparticle diffusion model, proposed by Weber and Morris, accounts for the possibility that diffusion of adsorbate molecules into the pores of the adsorbent may control the overall rate of adsorption [11]. The model is described by the following relation in Equation 8:

$$q_t = K_{id} t^{1/2} + C_t \quad \text{(S8)}$$

Where, K_3 (mg/g·hr$^{1/2}$) is the intraparticle diffusion rate constant and C_t (mg/g) is the intercept reflecting the boundary layer thickness in the intraparticle diffusion model equation. A larger C_t value indicates a stronger boundary layer effect, while a straight line passing through the origin suggests that intraparticle diffusion is the sole rate-controlling step. In most cases, multi-linearity in the plots indicates multiple stages of adsorption, such as external surface adsorption followed by intraparticle diffusion.

S.5. FESEM-EDX Data

S.5.2. FESEM-EDX for Sandstone

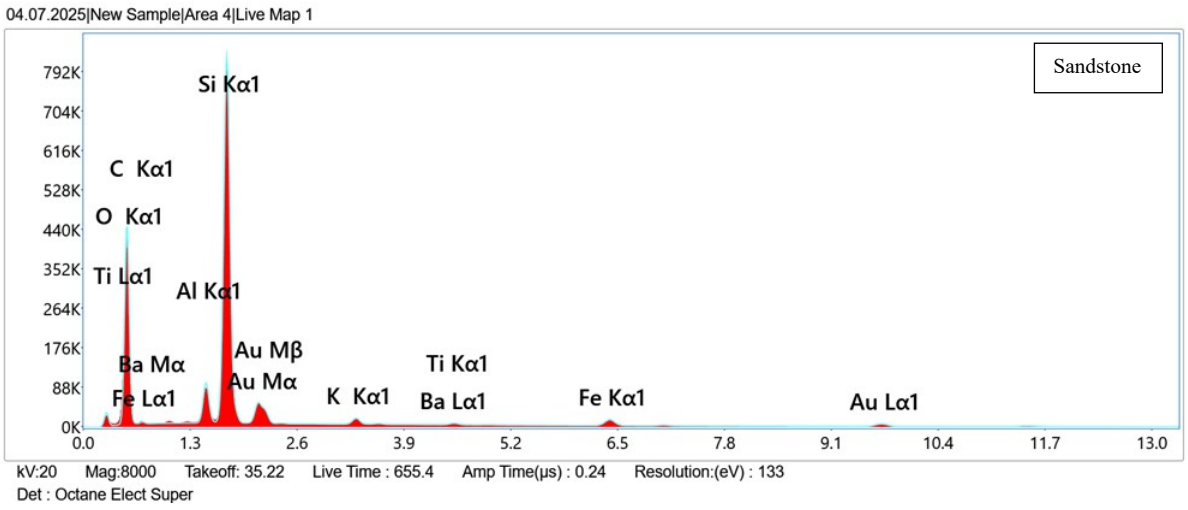

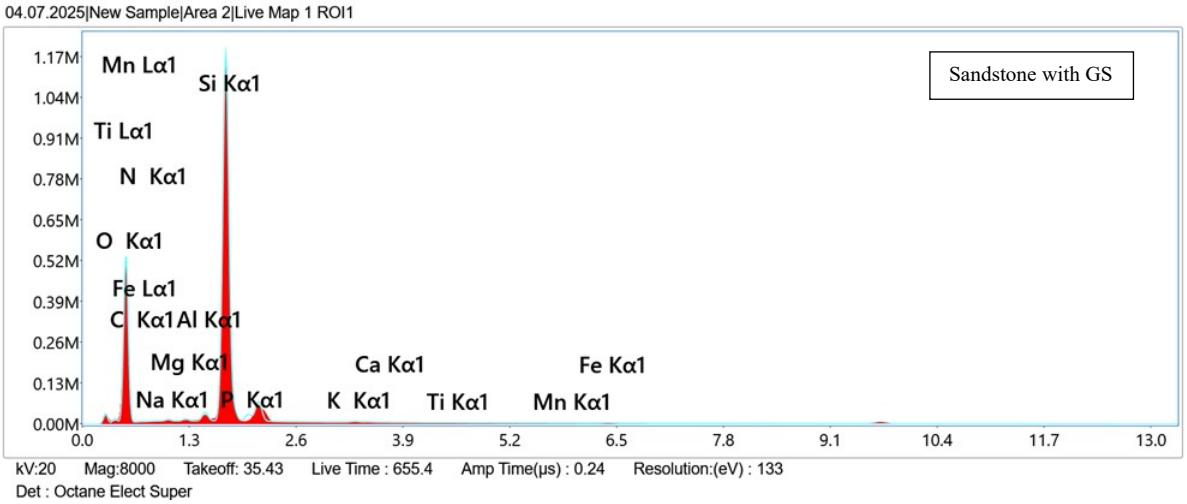

Fig. S2: Elemental peaks of sandstone components showing in EDAX

Table S2: Elemental Analysis of the Sandstone Rock Sample with and without Surfactant

Element	Weight %	
	Sandstone without Hexamine GS	Sandstone with Hexamine GS
C	15.5	18.9
N	0.0	3.1
O	46.1	50.2
Na	0.5	0.2
Mg	0.3	0.2
Al	3.9	1.5
Si	35.1	25.6
P	1.3	0.8
K	1.1	0.2
Ca	0.1	0.1
Ti	0.5	0.1
Fe	2.9	0.5

S.5.2. FESEM-EDX for Carbonate

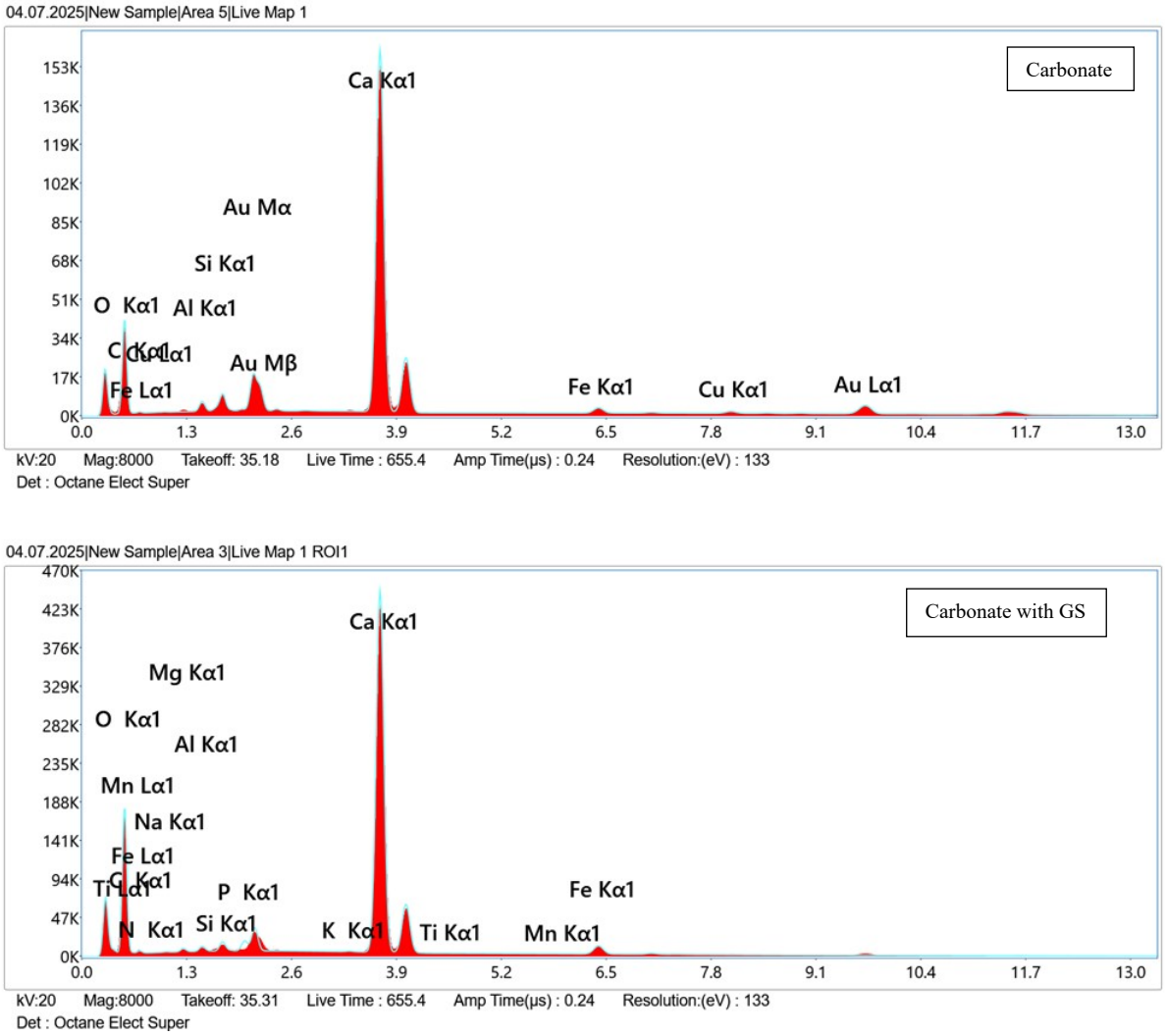

Fig. S3: Elemental peaks of carbonate components showing in EDAX

Table S3: Elemental Analysis of the Carbonate Rock Sample with and Without Surfactant

Element	Weight %	
	Carbonate without Hexamine GS	Carbonate with Hexamine GS
C	18.2	19.5
N	0.0	2.7
O	44.2	46.4
Mg	0.2	0.1
Al	0.7	0.2
Si	1.2	0.2
P	1.1	0.4
K	0.5	0.1

Ca	47.5	32.5
Fe	1.8	1.6
Cu	1.7	1.0

S.6. Adsorption with Prolonged Time

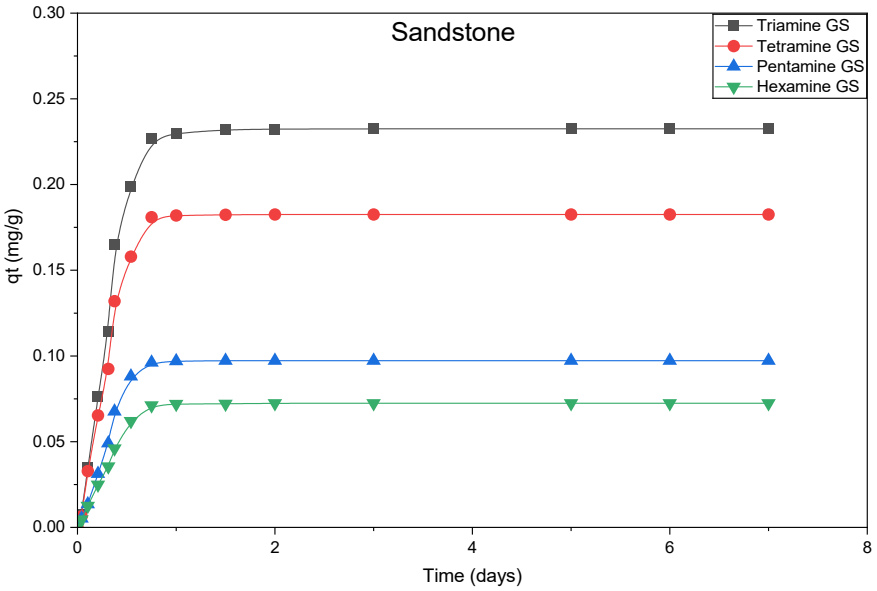

Fig. S4: Adsorption behaviour of Gemini surfactants on sandstone rock sample over prolonged contact time.

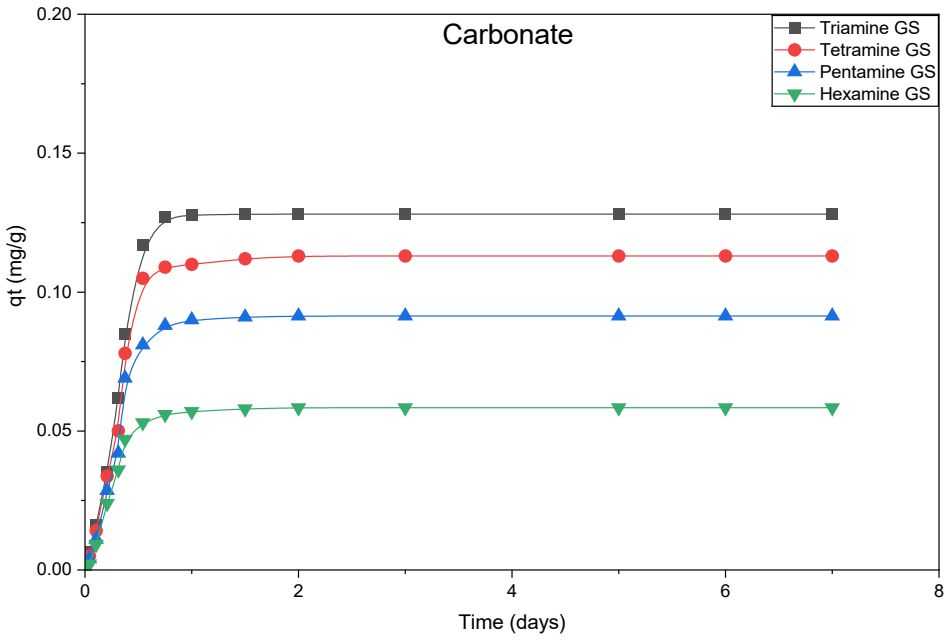

Fig. S5: Adsorption behaviour of Gemini surfactants on carbonate rock sample over prolonged contact time.

References:

1 A. Isah, M. Arif, A. Hassan, M. Mahmoud and S. Iglauer, *Energy Reports*, 2022, 8, 6355–6395.
2 N. Saxena, S. Kumar and A. Mandal, *Asia-Pacific J Chem Eng*, 2018, 13, e2211.
3 S. Kalam, S. A. Abu-Khamsin, M. S. Kamal, S. M. S. Hussain, K. Norrman, M. Mahmoud and S. Patil, *Energy Fuels*, 2022, 36, 5737–5748.
4 M. P. Mubiayi, 2014.
5 S. Kalam, S. A. Abu-Khamsin, A. O. Gbadamosi, S. Patil, M. S. Kamal, S. M. S. Hussain, D. Al-Shehri, E. W. Al-Shalabi and K. K. Mohanty, *Sci Rep*, 2023, 13, 11936.
6 I. Langmuir, *J. Am. Chem. Soc.*, 1916, 38, 2221–2295.
7 H. M. F. Freundlich, *J. Phys. chem*, 1906, 57, 1100–1107.
8 K. Y. Foo and B. H. Hameed, *Chemical Engineering Journal*, 2010, 156, 2–10.
9 L. K. Koopal, W. H. Van Riemsdijk, J. C. M. De Wit and M. F. Benedetti, *Journal of Colloid and Interface Science*, 1994, 166, 51–60.
10 E. D. Revellame, D. L. Fortela, W. Sharp, R. Hernandez and M. E. Zappi, *Cleaner Engineering and Technology*, 2020, 1, 100032.
11 W. J. Weber and J. C. Morris, *J. Sanit. Engrg. Div.*, 1963, 89, 31–59.
12 S. LAGERGREN, *K. Sven. Vetenskapsakad. Handl.*, 1898, 24, 1–39.
13 H. Wang, A. Zhou, F. Peng, H. Yu and J. Yang, *Journal of Colloid and Interface Science*, 2007, 316, 277–283.